doi:10.3723/WCYG1090

A load-transfer curve formulation to predict the drained response of offshore piles to pull-out

G. Orlando, L. Govoni & R. Zabatta
University of Bologna, Bologna, Italy

A. Foglia
Fraunhofer Institute for Wind Energy Systems IWES, Hannover, Germany
Currently Norwegian Geotechnical Institute, Oslo, Norway

ABSTRACT: The study introduces a formulation for load-transfer curves ($t-z$) to predict the load-displacement behaviour of offshore steel piles subjected to axial tensile loading. This condition is particularly relevant to foundations for wind turbines in intermediate to deep water, supporting jackets or anchoring floating structures. The problem is first addressed using a continuum approach implemented with the finite element method. Interface behaviour is modelled using the results of interface tests. Available data from pile tests, featuring different geometries, are used to assess the model ability to reproduce the experimentally observed response. The results of the finite element analyses are then used to develop and calibrate $t-z$ curves, which are implemented in a simpler one-dimensional finite element model. The comparison of the results of the two-dimensional and one-dimensional approaches shows good agreement. It is also shown that the one-dimensional approach can be successfully implemented using the equations of the recently developed unified CPT method.

1 Introduction

Offshore pile foundations are traditionally used to support jackets for oil and gas facilities, but, when dealing with lighter structures such as wind turbines, tensile load can be particularly onerous.

Monopiles are the most widely used substructure for wind turbines installed in water depths of 25−30m, they transfer horizontal loads and overturning moments to the soil via lateral interaction. Historically, $p-y$ curves have been largely used in design practice (more recently, Jeanjean, 2017; Taborda, 2020).

Jackets on piles are suitable for water depths ranging between 30−60m, as for all other tripod structures, they transfer the overturning moment to the competent soil through a "push and pull" mechanism and, therefore, evaluation of the tensile bearing capacity of the soil is crucial.

Axial load-transfer $t-z$ curves, for deep slender piles, have long been studied (more recently, Wang, 2012; Nanda and Patra, 2014; Bohn, 2017).

This study proposes the evaluation of axial load-transfer curves to pull-out calibrated via a two-dimensional axisymmetric Finite Element (FE) model. The methodology proposed relies on the definition and assessment of interface behaviour, calibrated on available interface test data. The selected mathematical form for the $t-z$ curves is that of the recently proposed within the Pile Soil Analysis (PISA) framework (Burd, 2020). A method to evaluate the function parameters is then suggested with reference to a case study. The parameters are established using the results of interface tests and the equations of the unified Cone Penetration Test (CPT) method (Lehane, 2020).

The strength of the proposed approach relies on the definition of the curve parameters that can be obtained from tests easily available to designers.

2 Numerical modelling of pile tests

To validate the method, this work uses the results of model pile tests which were carried out at a "technical scale" of about 1:10 to 1:5, at the Test Centre for Support Structures of the Leibniz University of Hannover, Germany, within the framework of the EU project IRPWind (Foglia, 2017). The test design and data interpretation were performed by Fraunhofer IWES.

Three piles with different geometries were chosen for this study, with details given in Table 1. The piles are open-ended, medium rough (centre-line average steel surface roughness R_a= 5μm) and driven in a medium dense soil sample (D_r = 74%). The soil is a uniformly graded siliceous sand with a mean particle size of D_{50}=0.36mm. Minimum and maximum void ratios are e_{min} =0.44, and e_{max} =0.83. These values were estimated in 2015 for sand particles with a grain

Table 1. Piles geometry.

Name	D [m]	L/D [-]	D/t [-]
Pile 1	0.273	20.9	54.6
Pile 3	0.356	16.0	56.4
Pile 4	0.356	18.8	56.4

density of 2.65g/cm^3. The sample was prepared by compaction of sand layers using directional plate compactors and then saturated. CPT tests were carried out prior and after piles installation at a minimum pile distance of three-diameters.

Installation was close to fully cored for all piles and pull-out was fully plugged. More details on the experimental campaign can be found in Schmoor, (2018).

For FE modelling, the commercial FE package Abaqus was used. In total, three axisymmetric dynamic-implicit FE simulations were carried out.

2.1 *Mesh geometry and boundary conditions*

For the mesh (Figure 1), 4-node bilinear axisymmetric quadrilateral elements (CAX4) were used with four integration points per element. Zero displacement boundaries were set at a distance of 15D from the pile shaft and 10D down the pile tip. The nodes along the external boundary were horizontally restrained, while the bottom edge was fully fixed.

A sensitivity analysis on mesh refinement was performed to balance the accuracy of the results and computational cost. A structured mesh was used for the pile. Elements had a width equal to D/40 and an aspect ratio (element height to element width) of 10.

For the soil, a free mesh was adopted up to a distance from the pile of 3D, replaced by a structured mesh from 3D to the domain boundaries. A thin column of elements of thickness $5D_{50}$ and aspect ratio 10 was inserted between the pile and soil. The value of $5D_{50}$ was chosen as a representative thickness after observations on shear band formation on experimental setups. Shear band is generally between five to ten D_{50}. However, for the medium rough piles and uniform sand, $5D_{50}$ appeared as a reasonable modelling choice (DeJong, 2006, Tovar-Valencia, 2018).

When using a free mesh, extremely distorted elements may cause convergence problems. The quality of generated elements was checked with the Abaqus diagnostic tool, which returns a warning for elements that seem inappropriately distorted and an error if the distortion is severe.

2.2 *Soil and pile modelling*

To simulate the behaviour of the soil, the Sanisand constitutive model (Dafalias and Manzari, 2004) was used. The sand parameters were calibrated on triaxial tests. In Figure 2a the model results are compared with the data obtained in isotropically consolidated

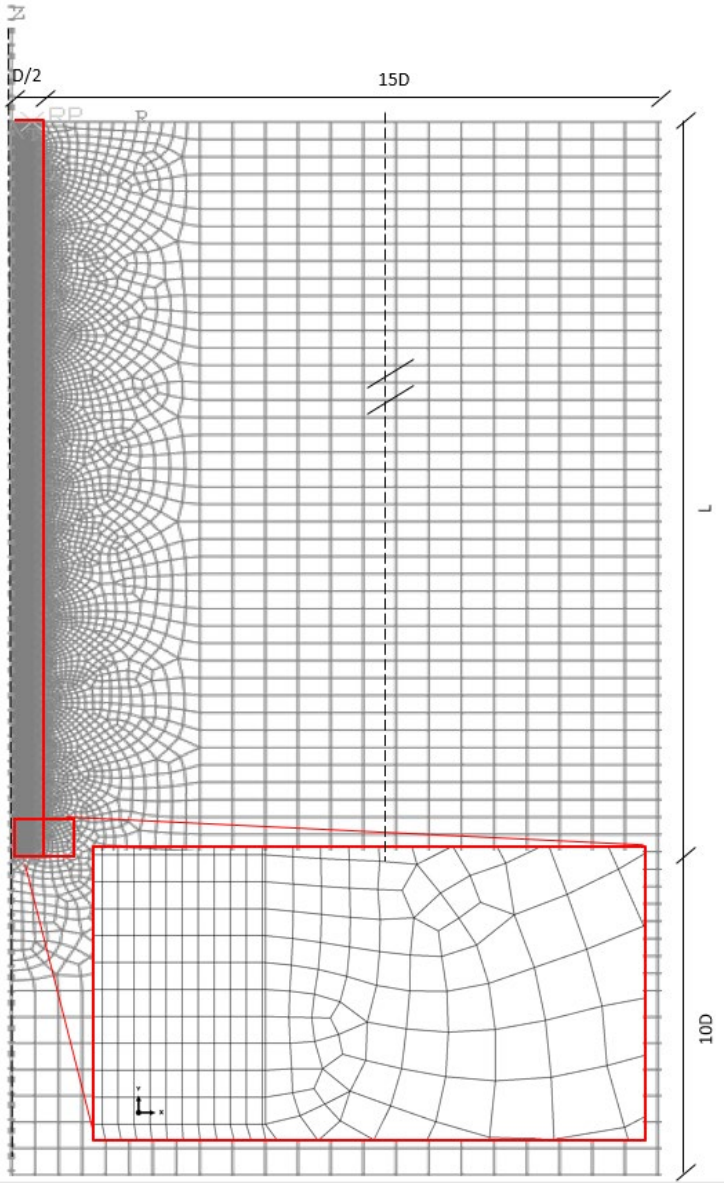

Figure 1. Finite Element pile mesh geometry. Interface elements of $5D_{50}$ are highlighted.

drained triaxial tests at three different levels of confining stress (30, 60, 90kPa). The critical state line in the $p-e$ plane is described by the parameters e_{c0}, λ and ξ that have been determined fitting the triaxial test results. Parameters M_c and M_e, instead, describe the critical state line on the $p-q$ plane for triaxial compression and extension respectively, computed using the critical friction angle determined from the triaxial tests (φ_{cv}=32.6°).

The parameter m represent the opening of the yield surface and the chosen value allow for a proper small-strain response. The shear modulus constant $\overline{G_0}$ was taken as best fit to the experimental initial stiffness.

As for Poisson's ratio, a low value of $\nu = 0.05$ is necessary for the Sanisand (2004) model to reproduce the experimental oedometric stiffness.

Plastic modulus parameters h_0, c_h and n_b were calibrated to properly reproduce the experimental results of the drained triaxial stress-strain response, while dilatancy parameters n_d and A_0 were chosen to reproduce the volumetric response.

Table 2. Sanisand (2004) parameters sets.

Sanisand (2004) parameters			Soil set	Interface elements set
Void Ratio on Critical state line at p=0	e_{c0}	[-]	0.620	0.620
CSL parameter (on p-e plane)	λ	[-]	0.015	0.015
CSL parameter (on p-e plane)	ξ	[-]	0.400	0.400
CSL (p-q plane) in TX compression	M_c	[-]	1.309	1.070
CSL (p-q plane) in TX extension	M_e	[-]	0.911	0.789
Opening of yield surface cone	m	[-]	0.020	0.020
Shear modulus constant	$\overline{G_0}$	[-]	200	5.000
Poisson's ratio	ν	[-]	0.050	0.050
Plastic modulus constant	h_0	[-]	5.000	5.000
Plastic modulus constant	c_h	[-]	0.968	0.968
Plastic modulus constant	n_b	[-]	1.400	0.800
Dilatancy constant	A_0	[-]	0.900	0.220
Dilatancy constant	n_d	[-]	2.500	3.500
Fabric-dilatancy tensor	c_z	[-]	0	0
Fabric-dilatancy tensor	z_{max}	[-]	0	0

Parameters z_{max} and c_z account for the cyclic effect, they were set to zero as in this study only monotonic conditions were investigated.

The calibrated parameters provided in Table 2 allowed for a good fitting of the experimental data in terms of both stress-strain and volumetric response (Figure 2a).

The piles were modelled as deformable linear-elastic steel piles. As the pile installation was close to fully cored and observed failure fully plugged, a uniform cross-section with equivalent density and mechanical properties were assigned to the pile.

Perfect contact was prescribed at the pile-soil interface, imposing that the shearing along the pile shaft occurred in the thin layer of soil, of thickness of $5D_{50}$, adjacent to the pile.

To these elements the Sanisand model (2004), was also prescribed, whose constants were adjusted using available experimental results of Constant Normal Load (CNL) interface tests. These tests involved medium densey samples of the sand used for pile tests and steel plates of average roughness R_a= 5μm; conditions which were created to reproduce those of model piles.

Figure 2b compares the experimental data, in continuous grey line, to the interface model prediction, in black lines. Interface results are presented with reference to the range of stress (30, 90kPa) and horizontal displacements (up to 8 mm) relevant to the pile application. The agreement is overall satisfactory, with some scatter shown at the lower confining stress, notably in the underestimation of the initial sample contraction, and strain softening. The model constants are also provided in Table 2.

Once calibrated, the interface FE model can be use to predict the interface response to other confining stresses (see Section 3).

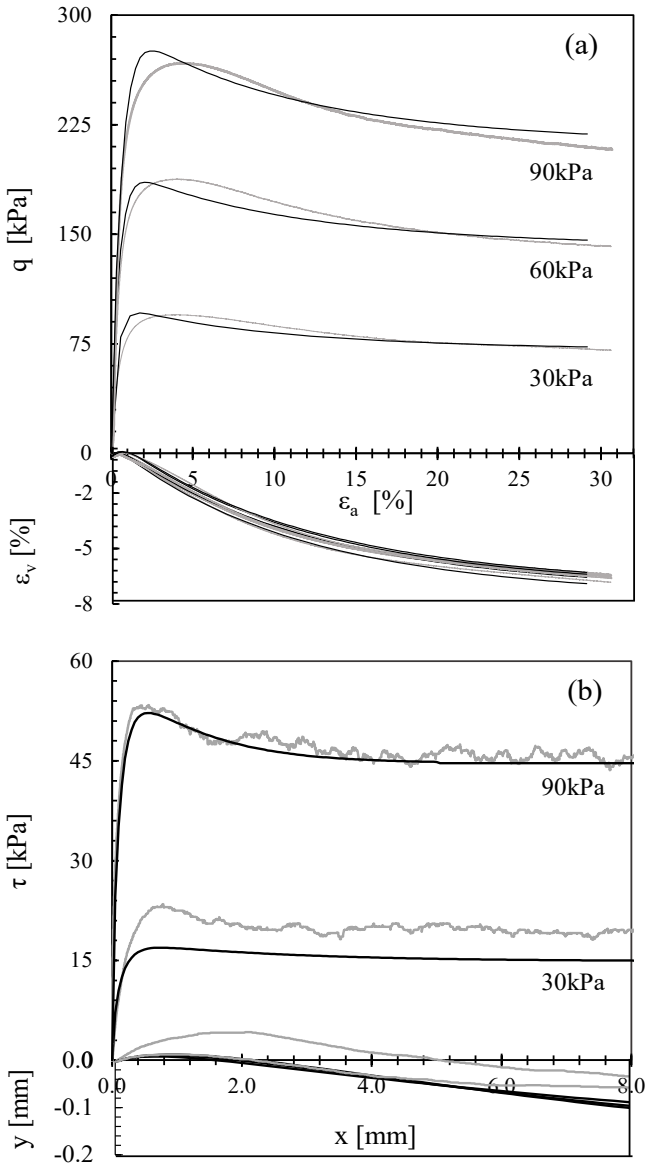

Figure 2. Calibration of soil and interface elements using Sanisand (2004): (a) soil model calibration based on triaxial tests and (b) interface calibration using available CNL interface tests.

The contact between the pile base and the soil was modelled as "hard" contact, not allowing for the transfer of tensile stresses across the interface.

2.3 *Initial conditions and loading stages*

Piles were whished-in-place. The aim of the work is to evaluate the pile response during loading phase, therefore, the initial stress state is calibrated to ensure the agreement between the increase of radial stresses during loading and those predicted by the CPT method (Figure 6b). It was verified that the extracted $t - z$ were in accordance with the predictions of the unified CPT method.

In absence of procedures to initialise the radial and circumferential stress variables within the soil domain, which do not involve FE modelling of the installation process, a uniform earth pressure coefficient K_a was assigned to soil domain.

On the experimental side, no specific measurements were made to this end and the CPTs, carried out prior and after the pile driving, showed no influence of pile installation at a three-diameter distance from the pile

The initial average earth pressure coefficient was taken equal to 0.8. The value was selected according to the suggestion of Tovar-Valencia (2018) as the one to be used for medium rough displacement piles in medium dense silica sand. The choice was based on the observed satisfactory match of the mobilised average unit shaft resistance of the IRPWind piles with those of the aforementioned testing campaign (Tovar-Valencia, 2018), which certainly bore similarities (e.g. materials, geometries) but also some discrepancies, notably, in the installation procedure.

The installation effects on the residual shear stresses, τ_{res}, were instead implemented following the approach proposed by Alawneh, (2001), which resulted in values of τ_{res}=5.17, 4.19, 4.29kPa, for Pile 1, 3, 4, respectively.

Following this step, an upward vertical displacement was assigned to the mode pile head up to the simulation end which corresponded to the achievement of ultimate conditions in all interface elements.

2.4 *FE results and discussion*

In Figure 3a, the numerical load-displacement curves for the three piles are presented against the experimental results, showing an excellent agreement up to the simulation.

Figure 3b shows the evolution of the radial confining stress, σ'_{rc}, with the shear stress, τ, for Pile 3 at selected, equally spaced, points along the shaft. The paths start from the assigned value of residual shear stress, then monotonically evolve to reach a unique failure line of inclination $\delta_{cv} = 27°$. The trend agrees to that observed in laboratory model pile tests in a clean siliceous sand sample, as reported by Lehane (1992). In the same research work, results of pile tests, carried out on site, were also shown in which the confining radial stress, first decreased then increase up to the failure line; an aspect that the FE model didn't capture. The response of the IRPWind pile tests was, however, expected to be closer to laboratory experiments on uniformly graded commercial sands, rather than site tests carried out in natural dense sands. In this light, the FE model outputs appear reasonable.

3 Development and calibration of t-z curves

The numerical load-transfer curves were extracted at the nodes of the interface elements and then averaged upon equally sized layers of 0.475m height, for a total of 12 curves. The procedure was followed for all three piles. Figure 4a display a selection of the curves for Pile 3.

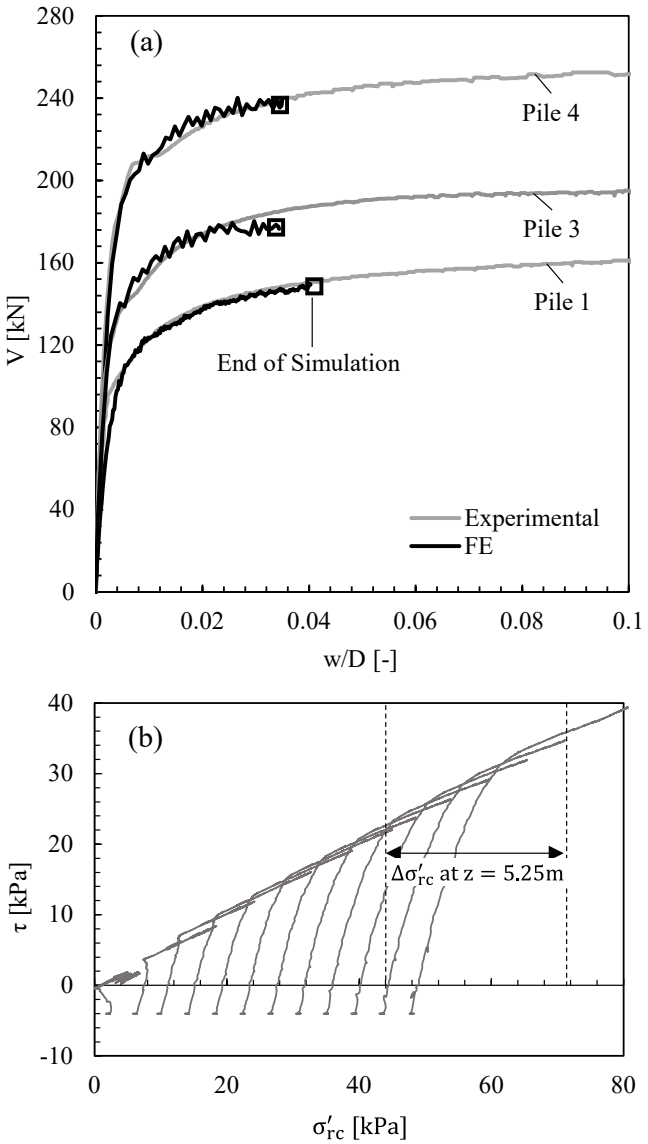

Figure 3. Results of simulation: (a) comparison of the FE load-displacements curves for the three piles and the experimental results and (b) stress path followed by the selected interface elements at Pile 3.

All curves show a hardening type of response, with the shear stress monotonically increasing up to the ultimate value, τ_u.

Such behaviour, characterised by no shear softening, is that expected along a constant normal stiffness stress paths, as it was also recently observed by Staubach (2022). Constant normal stiffness conditions are commonly acknowledged to be close (although not precisely so) to that experienced by the soil along the shaft of axially loaded piles. In fact, the numerical path followed by interface elements on the pile, differs from that observed both experimentally and numerically in CNL conditions, in which a peak shear stress is clearly mobilised (Figure 2b).

The load-transfer curves divided by the mobilised radial confining stress, σ'_{rc}, revealed to be in a good agreement with the shear stress-horizontal displacement curves obtained from CNL interface tests, normalised by the applied normal stress. This agreement is shown in Figure 4b, where all normalised load-transfer curves are plotted along with the results of interface tests.

These tests were carried out numerically, using the constants of Table 2 for interface elements and assigning, as normal stress, the initial radial confining stress level, acting at the location of the load-transfer curves (i.e. the initial radial confining stress $\sigma'_{rc,i}$ on the pile shaft).

The agreement is overall good in terms of initial shear stiffness, mobilised interface friction angle and displacements and provide the basis for the determination of load-transfer curves parameters as described in Section 3.1.

3.1 *Formulation of t-z curves*

The extracted FE load transfer curves were then normalised as indicated in Table 3.

The vertical displacement w was divided by the ratio between the shear band thickness $5D_{50}$ and the normalised surface roughness $R_n = R_a/D_{50}$. The thickness of the shear band is assumed to be only function of D_{50} and to be the same along the pile shaft and in interface tests. This normalisation allows to pursue the analogy between the load-transfer curves and the interface test results, also enabling to account for the pile roughness. In this study medium rough piles were considered, but the procedures could be assessed on different roughness and then framework extended to encompass more cases.

Table 3. Normalisation for $t-z$ curves

Normalised Variable	Normalisation
Shear stress, $\bar{t}$	$\frac{\tau}{\sigma'_{rc,i}}$
Vertical upward displacement, $\bar{w}$	$\frac{wR_n}{5D_{50}}$

The mobilised shear stress was instead divided by the initial radial confining stress $\sigma'_{rc,i}$.

The functional form given to the curves was the second-degree conical function recently adopted within the PISA framework (Byrne, 2020):

$$-n\left(\frac{\bar{t}}{\overline{t_u}}-\frac{\bar{w}}{\overline{w_u}}\right)^2+(1-n)\left(\frac{\bar{t}}{\overline{t_u}}-\frac{\bar{w}G}{\overline{t_u}}\right)\left(\frac{\bar{t}}{\overline{t_u}}-1\right)=0 \qquad (1)$$

where $\bar{t}$, and $\bar{w}$, are, respectively, the normalised shear stress and upward displacement, $\overline{t_u}$ is the ultimate normalised shear stress, $\overline{w_u}$ is the normalised displacement at which the ultimate shear stress is reached, G is the initial slope of the curve and n, with $0 \le n \le 1$, defines the curvature.

3.1.1 *Parameters definition and estimation*

The ultimate normalised shear stress $\overline{t_u}$ was computed as:

$$\overline{t_u}=\frac{\tau_u}{\sigma'_{rc,i}}=\frac{\sigma'_{rc,f}}{\sigma'_{rc,i}}\tan(\delta_{cv}) \qquad (2)$$

where $\sigma'_{rc,f}$ is the effective radial confining stress at failure. The constant volume friction angle δ_{cv} was determined from interface tests as shown in Figure 4b, while $\sigma'_{rc,f}$ was expressed as linear function of the normalised depth z/L as follows

$$\sigma'_{rc,f}=a\frac{z}{L}+b \qquad (3)$$

where a, and b are constants, obtained as best fit of the equation to FE load-transfer curves, using the least square approach (error < 3.1%).

Therefore, $\overline{t_u}$ can be rewritten as:

$$\overline{t_u}=\frac{\sigma'_{rc,f}}{\sigma'_{rc,i}}\tan(\delta_{cv})=\frac{\tan(\delta_{cv})}{\sigma'_{rc,i}}\left(a\frac{z}{L}+\mathrm{b}\right) \qquad (4)$$

The ultimate normalised displacement $\overline{w_u}$ is taken as the value at which $\tau/\sigma'_{rc}=\tan(\delta_{cv})$, as illustrated in Figure 4b.

The initial slope of the load-transfer curve can be expressed as function of $\sigma'_{rc,f}$ as follows:

$$G=\frac{k}{\sigma'_{rc,i}}\left(a\frac{z}{L}+\mathrm{b}\right) \qquad (5)$$

where k is a dimensionless constant. The interpolation of the first linear portion of the FE load-transfer curves gave a k = 610, a value close to that obtained using the interface tests data only (k = 640, being $\sigma'_{rc}\sim\sigma'_{rc,i}$ at the initial branch of the curve).

The curvature n was evaluated equal to 0.84 following a non-linear fitting of all FE load-transfer curves using the Gauss-Newton non-linear least square approach (error < 2%), and equal to 0.9 (error < 6%) using the interface tests data.

The load transfer curves constants are provided in Table 4, referring to the source used for their estimation.

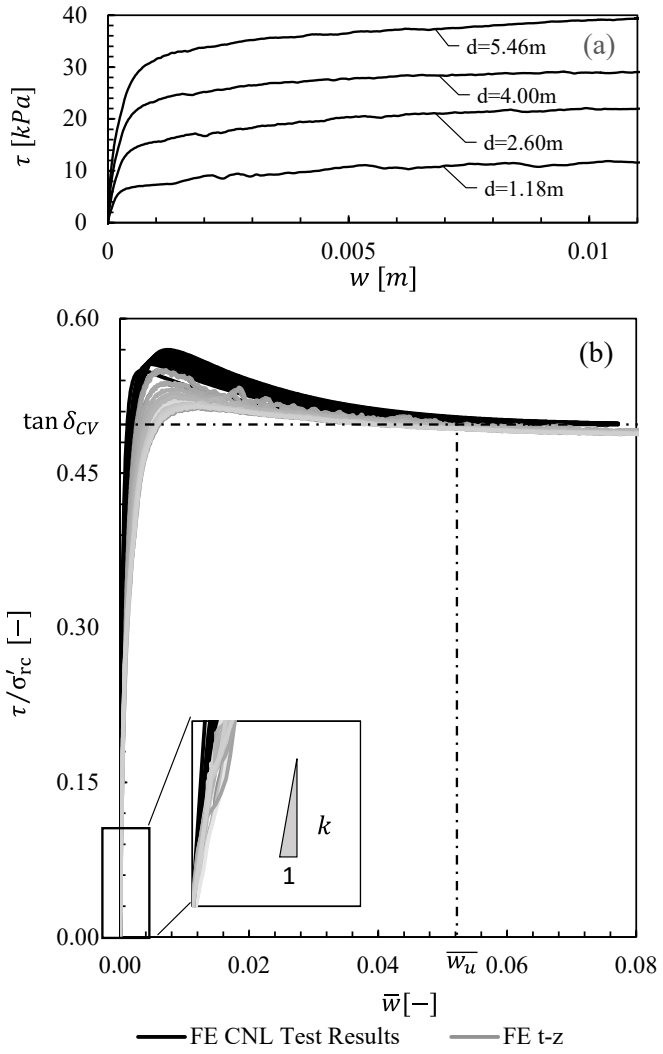

Figure 4. Development of shaft load-transfer curves: (a) selection of extrapolated FE $\tau - w$ curves presented without normalisation, (b) normalised FE $t - z$ curves compared against CNL interface test results, with an indication of how to infer the model parameters.

3.2 *Implementation of the load-transfer curve in one-dimensional FE model*

The load-transfer curves were implemented in a one-dimensional FE model. For the pile, truss elements were used with the density and axial stiffness already prescribed in the two-dimensional model.

The soil was modelled with non-linear springs of response described by Equation 1, using the constant determined from interface tests, illustrated in Table 4 and ultimate capacity obtained from the numerical load-transfer curves computed with Equation 4. The model also implements the residual stresses following the estimation of Section 2.3.

Table 4. 1D model parameter sets

1D Parameters	from FE $t - z$	from interface tests
a	78.140	-
b	9.080	-
$\tan(\delta_{cv})$	0.510	-
$\overline{w_u}$	0.055	0.055
k	610	640
n	0.840	0.900

The load-displacement curves of the one-dimensional and two-dimensional models are shown in Figure 5, displaying an overall satisfying agreement.

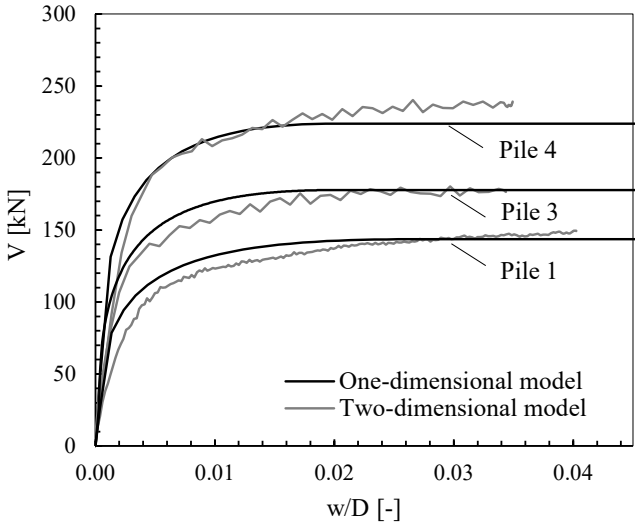

Figure 5. Comparison between the 1D $t - z$ model and 2D FE model.

3.3 *Use of the unified CPT framework*

The implementation of the load-transfer curves could be completed using interface shear tests data in combination with the unified CPT method (Lehane, 2020). Therefore, the proposed formulation of t-z curves is independent from the results of two-dimensional FE analyses. The CPT method would enable for the estimation of the ultimate shear stress $\overline{t_u}$, provided that relevant cone tip resistance data are available.

The ultimate shear stress, as expressed in Lehane (2020), normalised by $\sigma'_{rc,i}$ is:

$$\overline{t_u} = \frac{\tau_u}{\sigma'_{rc,i}} = 0.75\left(1 + \frac{\Delta\sigma'_{rc,f}}{\sigma'_{rc,i}}\right)\tan 29° \quad (6)$$

with:

$$\Delta\sigma'_{rc,f} = \left(\frac{q_c}{10}\right)\left(\frac{q_c}{\sigma'_{v0}}\right)^{-0.33}\left(\frac{d_{CPT}}{D}\right) \quad (7)$$

where $\Delta\sigma'_{rc,f}$ is the increment of confining radial stress computed at the pile pull-out, d_{CPT} is the diameter of the CPT cone, D is the pile diameter and q_c is the tip resistance. The initial radial confining stress is computed as:

$$\sigma'_{rc,i} = \frac{q_c}{44}\left[1 - \left(\frac{D-2t}{D}\right)^2\right]^{0.3}\left[\max\left(1, \frac{L-z}{D}\right)\right]^{-0.4} \quad (8)$$

The q_c profile next to the pile locations, calculated averaging the results of five CPTs (Schmoor, 2018) is given in Figure 6a. The profile was used to calculate $\Delta\sigma'_{rc,f}$ according to Equation 7, for the three piles and results are presented in Figure 6b. Since Pile 3 and Pile 4 share the same diameter, they overlap up to L/D = 18.8, while Pile 1 has the smaller diameter resulting into slightly larger radial stresses.

The empirically derived curves are compared with the FE predictions, which were calculated as schematically illustrated in Figure 3b, with reference to Pile 3.

The FE and CPT based profiles are in close agreement. In fact, the one-dimensional model which implements Equation 1, with interface parameters of Table 4 and $\bar{t_u}$ as per Equation 6 provide a close match to the experimental results.

Please note that, when implementing the CPT method for estimating the ultimate capacity the expression of initial radial confining stress should be computed as per Equation 8.

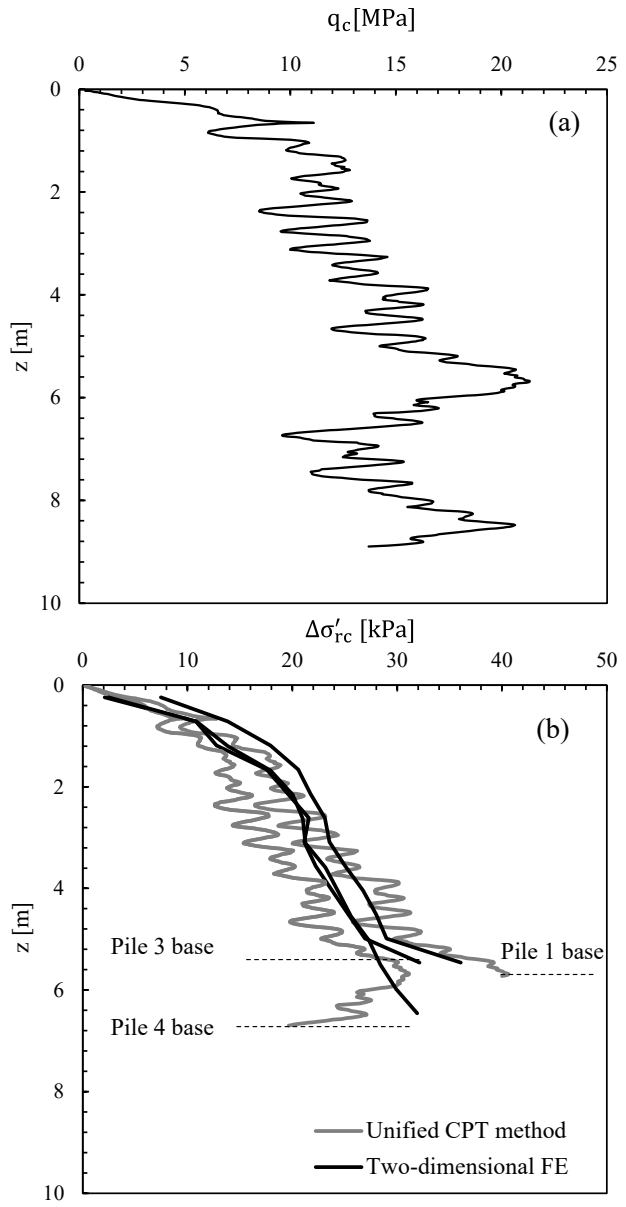

Figure 6. (a) Average CPT profile used. (b) Comparison between numerical $\Delta\sigma'_{rc}$ (in black) and the one computed with the unified CPT method (in grey).

Figure 7 shows the comparison between the experimental results of the IRPWind test campaign and the one-dimensional model with parameters estimated with interface CNL tests and the normalised ultimate shear stress calculated according to Equation 6, using the empirical approach of the unified CPT method. Specifically, Figure 7a, 7b, 7c show the numerical and experimental load-displacement curves for Pile 1, Pile 3 and Pile 4 respectively. It can be seen in Figure 7b where, for Pile 3, results were compared also with the $t-z$ prescribed by DNV-RP-C212 (2019), the proposed approach allows for the modelling of initial non-linearity and the estimation of ultimate displacement.

These results were obtained assuming that installation was fully cored for all piles consistently with the two-dimensional modelling choice. The results are in good agreement in terms of initial stiffness, non-linearity, ultimate displacement and ultimate capacity. This, combined with the agreement between the two-dimensional approach and of the unified CPT prediction of total ultimate radial stress increment during loading (Figure 6b), confirms the choice of the initial earth pressure coefficient in the two-dimensional model, as an average of the higher radial initial confining stress along the pile shaft and the far away soil, is substantially unaffected by installation.

The results show that $t-z$ curves can be calculated and implemented using the data from CNL interface if CPT data are available for the use of the unified CPT method.

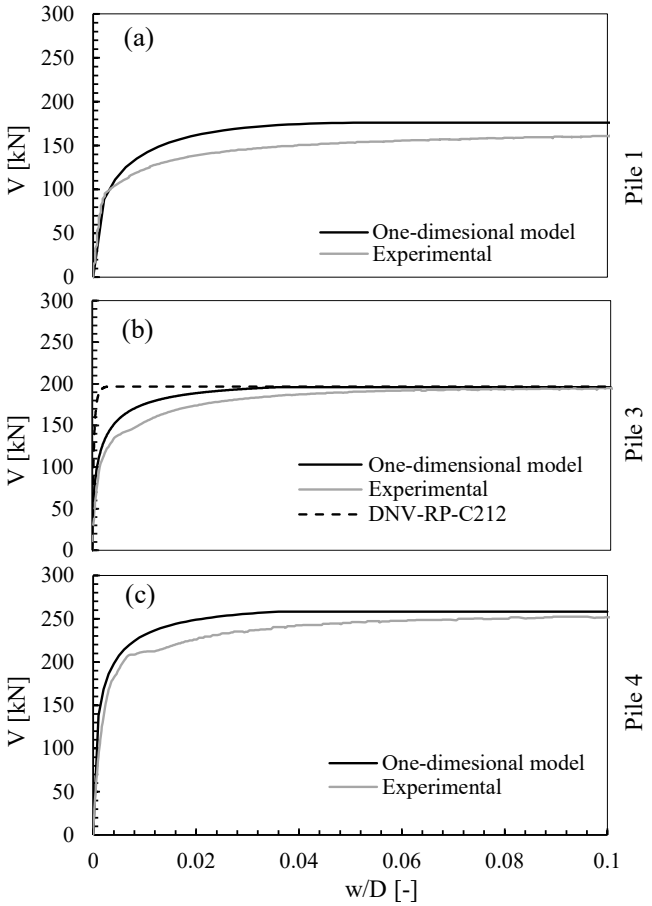

Figure 7. (a), (b), (c) Comparison of results between 1D model, using the CPT methods and interface test parameters, and the experimental results. For Pile 3 in Figure 7 (b), the results were compared also with t-z provided in DNV-RP-C212 (2019).

4 Concluding remarks

The following article has proposed a formulation for shaft load-transfer curves for steel piles subjected to axial tensile load and the procedure to determine its model parameters.

For the development and calibration of the procedure, "technical scale" model pile tests have been used in combination with a "gap-filling" FE model which was devised to allowed for the extraction of $t - z$ curves.

The mathematical form given to the curves is a second-degree conical function, dependent on the normalised shear stress, $\bar{t}$, and on the normalised upward displacement $\overline{w}$, with four parameters ($\overline{t_u}$, $\overline{w_u}$, n, k). The normalised ultimate displacement $\overline{w_u}$, the curvature n, and the initial slope coefficient, k, can be determined from constant normal load CNL interface tests, pursuing the analogy of load-displacement paths followed by sample in interface tests and the response observed at the pile interface.

The normalised ultimate shear stress, $\overline{t_u}$, can be computed using the recently proposed unified CPT method, which also provide a robust prediction of the initial radial confining stress $\sigma_{rc,i}$, which should be used as representative of real scale conditions.

The proposed approach allows to model initial non-linearity and to predict with great accuracy the ultimate displacement. Moreover, curve parameters can be obtained from tests easily available to designers.

This work is a preliminary study that requires further verifications on large-scale pile and on different soils, such as natural deposits, as well as observation of the effects of varying the pile normalised roughness.

5 Acknowledgment

The authors would like to thank the scientific staff of SoilModels (soilmodels.com) for providing the Abaqus subroutine used in this work.

6 References

Alawneh, A. S., Nusier, O., Malkawi, A. I. H. & Al-Kateeb, M. 2001. Axial Compressive Capacity Of Driven Piles In Sand: A Method Including Post-Driving Residual Stresses. *Canadian Geotechnical Journal,* 38**,** 364-377.

Bohn, C., Santos, A. L. D. & Frank, R. 2017. Development Of Axial Pile Load Transfer Curves Based On Instrumented Load Tests. *Journal Of Geotechnical And Geoenvironmental Engineering,* 143**,** 04016081.

Burd, H. J., Taborda, D. M. G., Zdravković, L., Abadie, C. N., Byrne, B. W., Houlsby, G. T., Gavin, K. G., Igoe, D. J. P., Jardine, R. J., Martin, C. M., Mcadam, R. A., Pedro, A. M. G. & Potts, D. M. 2020. Pisa Design Model For Monopiles For Offshore Wind Turbines: Application To A Marine Sand. *Géotechnique,* 70**,** 1048-1066.

Byrne, B. W. 2020. Editorial: Geotechnical Design For Offshore Wind Turbine Monopiles. *Géotechnique,* 70**,** 943-944.

Dafalias, Y. F. & Manzari, M. T. 2004. Simple Plasticity Sand Model Accounting For Fabric Change Effects. *Journal Of Engineering Mechanics,* 130**,** 622-634.

Dejong, J. T., White, D. J. & Randolph, M. F. 2006. Microscale Observation And Modeling Of Soil-Structure Interface Behavior Using Particle Image Velocimetry. *Soils And Foundations,* 46**,** 15-28.

DNV-RP-C212. Offshore soil mechanics and geotechnical enigineering. Recommended practice. Edition 2019-09-Amended 2021-09.

Foglia, A., Wefer, M. & Forni, F. 2017. Large-Scale Experiments And Load Transfer Analysis Of Piled

Foundations Supporting An Offshore Wind Turbines. *Proc. Int. Conf. Offshore Site*

Investigation And Geotechnics Osig 2017 London: Society For Underwater Technology.

Jeanjean, P., Zhang, Y., Zakeri, A., Andersen, K., Gilbert, R. & Senanayake, A. A Framework For Monotonic P-Y Curves In Clays. Proceedings Of The 8th International Conference, Osig 2017, 2017 London. The Society For Underwater Technology.

Lehane, B. 1992. *Experimental Investigations Of Pile*

Behaviour Using Instrumented Field Piles. Doctor Of Philosophy In The Faculty Of Engineering., University Of London.

Lehane, B., Liu, Z., Bittar, E., Nadim, F., Lacasse, S., Jardine, R. J., Carotenuto, P., Jeanjean, P., Rattley, M., Gavin, K., Haavik, J. & Morgan, N. 2020. A New 'Unified' Cpt-Based Axial Pile Capacity Design Method For Driven Piles In Sand. *4th International Symposium On Frontiers In Offshore Geotechnics.* Usa: American Society Of Civil Engineers.

Nanda, S. & Patra, N. R. 2014. Theoretical Load-Transfer Curves Along Piles Considering Soil Nonlinearity. *Journal Of Geotechnical And Geoenvironmental Engineering,* 140**,** 91-101.

Schmoor, K. A., Achmus, M., Foglia, A. & Wefer, M. 2018. Reliability Of Design Approaches For Axially Loaded Offshore Piles And Its Consequences With Respect To The North Sea. *Journal Of Rock Mechanics And Geotechnical Engineering,* 10**,** 1112-1121.

Staubach, P., Machaček, J. & Wichtmann, T. 2022. Novel Approach To Apply Existing Constitutive Soil Models To The Modelling Of Interfaces. *International Journal For Numerical And Analytical Methods In Geomechanics,* 46**,** 1241-1271.

Taborda, D. M. G., Zdravković, L., Potts, D. M., Burd, H. J., Byrne, B. W., Gavin, K. G., Houlsby, G. T., Jardine, R. J., Liu, T., Martin, C. M. & Mcadam, R. A. 2020. Finite-Element Modelling Of Laterally Loaded Piles In A Dense Marine Sand At Dunkirk. *Géotechnique,* 70**,** 1014-1029.

Tovar-Valencia, R. D., Galvis-Castro, A., Salgado, R. & Prezzi, M. 2018. Effect Of Surface Roughness On The Shaft Resistance Of Displacement Model Piles In Sand. *Journal Of Geotechnical And Geoenvironmental Engineering,* 144**,** 04017120.

Wang, Z., Xie, X. & Wang, J. 2012. A New Nonlinear Method For Vertical Settlement Prediction Of A Single Pile And Pile Groups In Layered Soils. *Computers And Geotechnics,* 45**,** 118-126.